Fraunhofer-Institut für Zerstörungsfreie Prüfverfahren IZFP

Campus E3 1
66123 Saarbrücken

Chair and Institute of Road, Railway and Airfield Construction
TUM School of Engineering and Design
Technical University of Munich

Arcisstr. 21
D-80333 München

Comet K-Project Rail4Future

Subproject 2.3

Condition Monitoring for predictive maintenance with smart assets – Smart Rail

D2.3.2
Report on Concept for Signal Evaluation and Signal Interpretation (M24)

Content

1. Design and Dimensioning of the Rail Test Rig and Preliminary Tests

For the preliminary studies, a test rig had to be invented in order to apply tensile and compressive force on a rail sample. With two hydraulic presses (each capable of 500 kN compressive force) and a relocatable crossbeam this requirement was met. The main operating principle can be seen in figure 1 and figure 2.

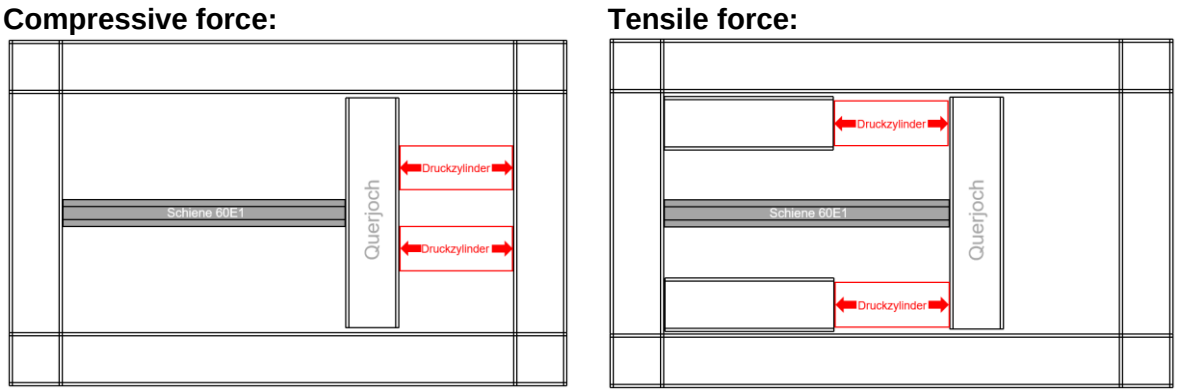

Figure 1: Main principle of the test rig in order to apply tensile and compressive force on a rail sample

A frame made of constructional steel (HEB 300) emerged as appropriate with regard to the required specifications (tensile and compressive forces of the two hydraulic presses ≈ 1 000 kN). In order to switch between compressive and tensile force introduction, the hydraulic presses and the supports have to be reversed, as can be seen in figure 2 and 3.

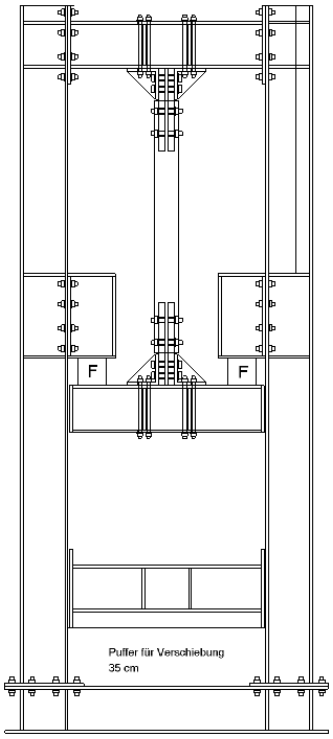

Figure 2: Technical drawing of the test rig for tensile force introduction

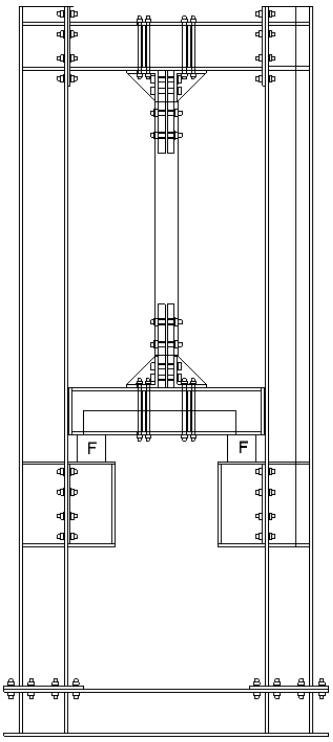

Figure 3: Technical drawing of the test rig for compressive force introduction

The mounting of the rail samples to the test rig frame had to meet special requirements: The test specimens have to be exchangeable within the test rig frame and tensile as well as compressive forces have to be applicable. For this purpose, the parts of an insulated rail joint (fishplates) were modified and mounted with massive angle sections, as can be seen in Figure 4.

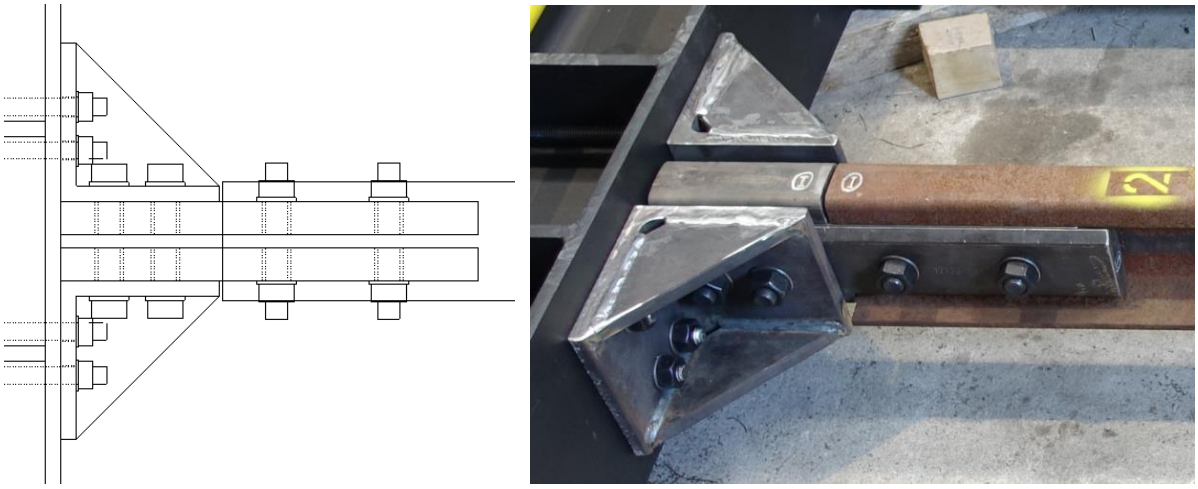

Figure 4: Technical drawing and mounting of the rail specimen

Preliminary studies were conducted with a short rail test specimen in order to figure out whether the load introduction is symmetrical and to preclude possible eccentricities of the load introduction.

For this, the rail specimen was prepared with 16 strain gauges in longitudinal direction of the rail. One exemplary strain gauge can be seen in Figure *5*. The attachment of the strain gauges was according to “DBS 918 254-01 Juli 2017” at two cross-sections of the test specimen. One cross-section in the middle of the rail test specimen, one cross-section 50 cm apart of it as comparison, as is depicted in Figure 5.

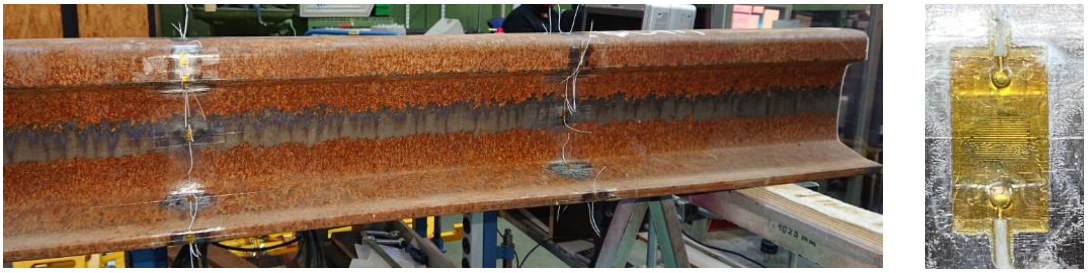

Figure 5: Short test specimen and example of an attached strain gauge

Figure 6: Mounted short test specimen loaded with compressive force

Exemplary values of the first tests with a compressive force of 700 kN are shown in Figure 7.

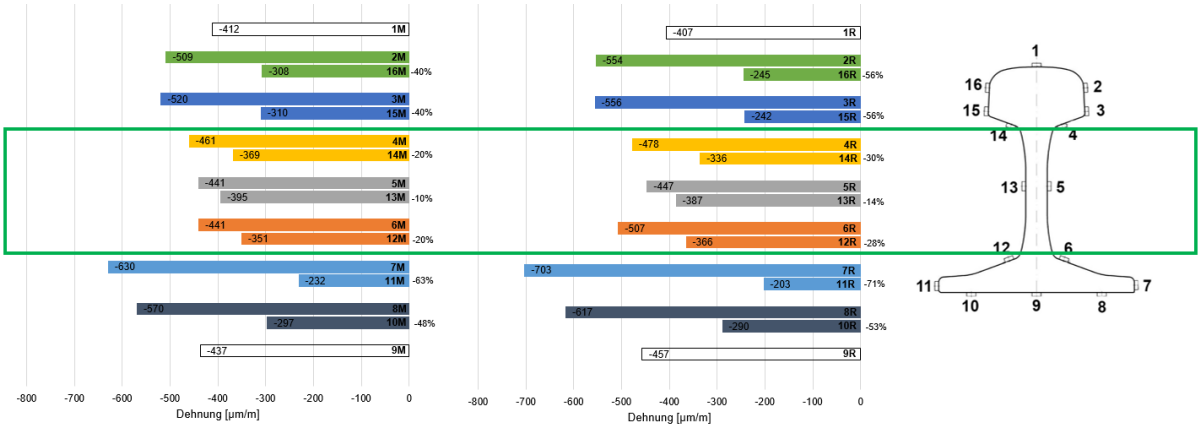

Figure 7: Exemplary strain values for a compressive force of 700 kN; green box resembles values of the rail web

By means of the first test, it was decided to extend the length of the test specimen. With this extension, it is possible to examine rail test specimens with an overall-length of 2.45 m. Less the mounting, the measurable length of a test specimen results to ~1.85 m.

2. Determination of the Methods for Monitoring the Load Stresses

Based on the results of the first year of the project and the analysis of the available methods and technologies already presented there, a selection of measurement principles was made, which were examined for suitability in preliminary tests.

The project consortium weighted the factors relevant to the process in order to achieve a high degree of suitability for use. The following prioritization was made:

1. interventions in the track position and the track bed are exclusion criteria.

2. usability on existing and new lines is decisive.

3. simplicity and low testing time < 3 minutes per position is critical.

4. integration independent of the solution into a test system is application critical.

5. discretization of test positions in the range of 10-50 meters is sufficient.

As a result, a selection was made of possible physical principles and measurement modalities which were subsequently tested after laboratory tests in the preliminary experiments on the hydraulic rail test rig of the TUM in order to plan the required measurements in the main experiments on the rail test rig.

The following physical principles will be the focus for the remainder of the project:

The following physical principles will be the focus for the remainder of the project:

1. Acoustic methods:

   These methods are based on structure-borne sound propagation and its acousto-elastic properties, regardless of the frequency range in the present project. The acousto-elastic effect is based on the fact that ultrasound is a compression wave passing through a material. It causes small deformations in the material's structure. These deformations can affect the way that the material propagates the compression wave, leading to changes in the wave's velocity. In turn, these changes in the wave's velocity can be used to measure the elastic properties of the material. By analyzing the changes in the sound velocity, it is possible to determine the material's elastic properties, such as its Young's modulus, Poisson's ratio, and shear modulus. The acousto-elastic effect can also be used to detect changes in the material's elastic properties due to external factors such as stress or temperature changes.

2. Magnetic methods:

   This technique involves applying a magnetic field to a material and measuring the electrical response of the material. The electrical response is caused by the induced electric currents that are generated in the material as a result of the changing magnetic field. By analyzing the electrical response, the magnetic permeability and electrical conductivity of the material can be determined. The behavior of magnetic materials under external stresses can be described by the Villari effect and the Joule effect. The Villari effect is a magnetostrictive effect that describes the change in magnetic permeability of a material when it is subjected to a mechanical stress. This effect can be observed in materials such as iron and nickel alloys, which exhibit an increase in magnetic permeability under compressive stress and a decrease in magnetic permeability under tensile stress. The Joule effect, on the other hand, describes the change in magnetic properties of a material due to a change in temperature. This effect can be observed in materials such as ferromagnetic alloys, which exhibit a change in their magnetic properties when they are heated or cooled.

3. Results of the Preliminary Tests

Several test approaches were investigated and evaluated on the first expansion stage of the rail test rig. Loads of 900 kN tensile force and 750 kN compression load were applied to the rail segment. The aim of this investigation was to evaluate the principle reproducibility, coupling conditions and the measurement effect. The following measurement modalities were used:

1. **Electromagnetically generated ultrasound - volume waves (acoustic approx. 2.3 MHz)**

   In this measurement, the ultrasonic transducer was placed laterally on the web and the time-of-flight differences of multiple reflections of two linearly polarized transverse waves were observed. The recording was made once parallel to the longitudinal direction of the rail and once perpendicular to it. Figure 8 shows an example of the displacement of the first backwall echo in the compression test.

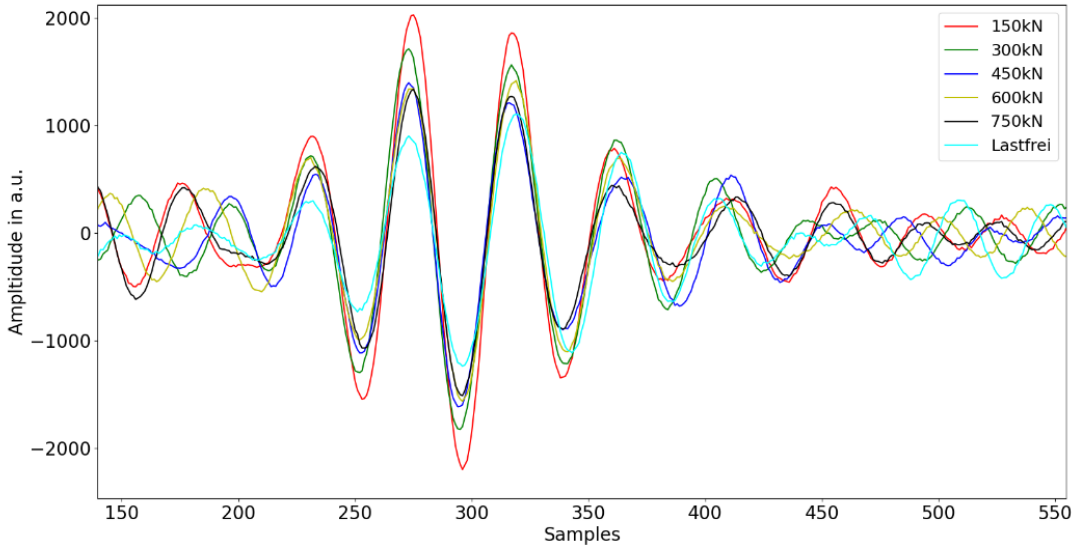

Figure 8: First backwall echo of ultrasonic testing perpendicular to the bar under compression load

This study shows that the change in ultrasonic time-of-flight is below resolvable technical limits due to the short travel distance with a hand-held system and the fluctuations due to lift-off and touchdown between load level-experiments.

2. **electromagnetically generated ultrasound - Rayleigh waves (acoustic < 500 kHz)**
   In this experiment, near-surface Rayleigh waves were sent through the web of the rail along the longitudinal direction of the rail in a transmitter-receiver arrangement. The radiated wave covers a distance of 150 mm and a time-of-flight evaluation is performed between the transmitted signal and the received echo. Figure 9 shows an example of the arrangement of the preliminary test.

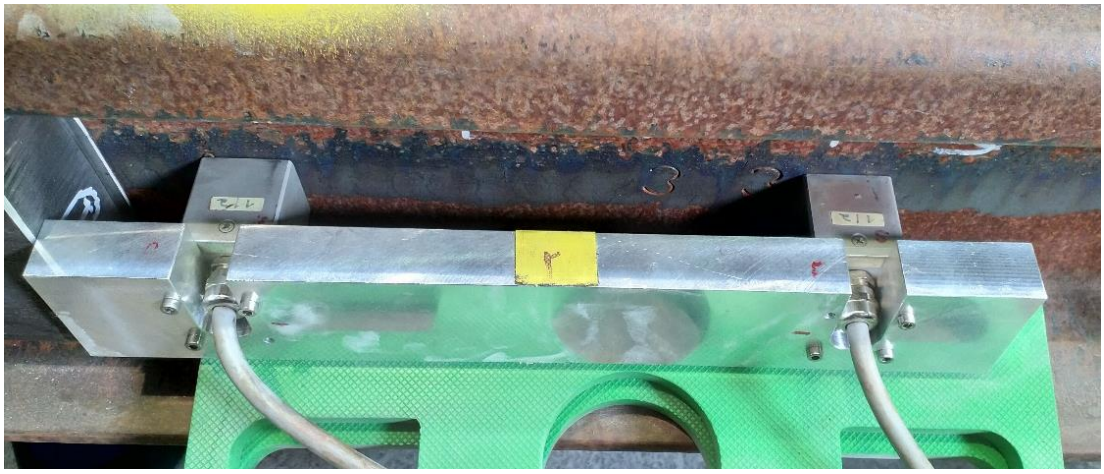

Figure 9: Transmitter-Receiver arrangement for Rayleigh wave measurement

This experiment could be performed exclusively with ultrasonic transducers for about 600 kHz transmission frequency. Although the generation of signal of low frequencies was necessary, there was no technical possibility to fulfill the limit condition for the generation of a pure SH0 mode of approx. 150 kHz. For this reason, superpositions of several wave modes appear in the resulting A-scans. At the frequency used, superimposed SH1 and SH2 components are present.

As a result, no reliable time-of-flight evaluation was possible. However, due to the expected low measurement effects of < 0.5 per mil and the extremely high costs of an adapted development, the necessary optimization within the project is not considered economical and not scientifically justified.

3. **Excitation of structure-borne sound (acoustic up to 20 kHz)**
   For the excitation of structure-borne vibrations in the web of the rail, the potential was first determined in the preliminary test to implement a reproducible mechanical excitation at a local measuring point under the applied loads and thus to draw possible conclusions about the longitudinal stress. For this purpose, a ceramic sphere with a defined drop height (Figure 10) was used for multiple excitation. The emitted structure-borne sound was recorded opposite the excitation point defined on the rail web.

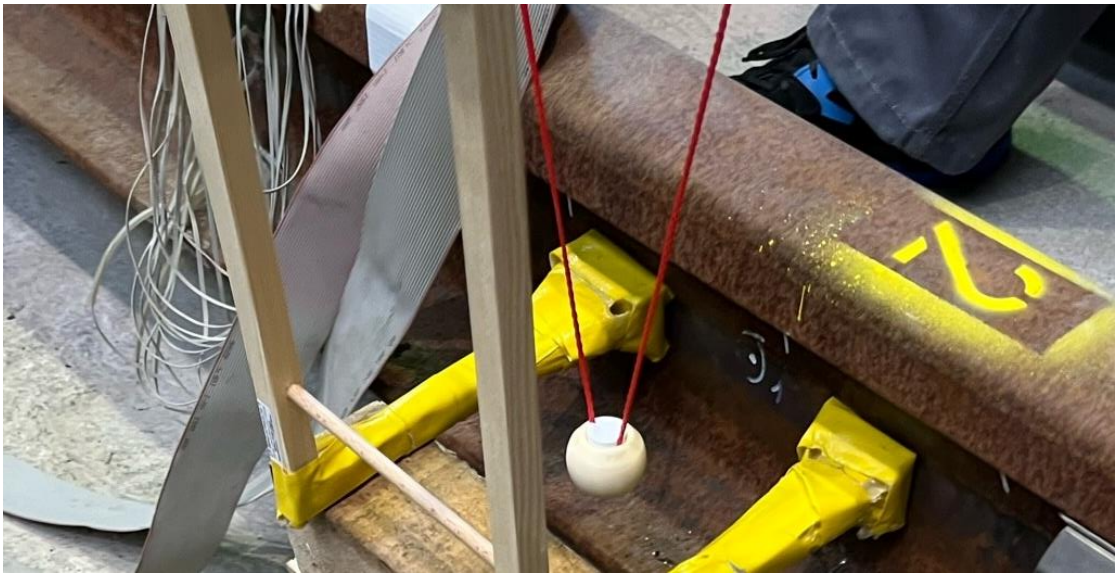

Figure 10: Test arrangement for multiple excitation

This results in the signals shown as an example in Figure *11* in the left diagram. These are representative of the recorded signals and can be evaluated on the basis of their characteristic decay times and set in relation to the load voltage (Figure *11* right).

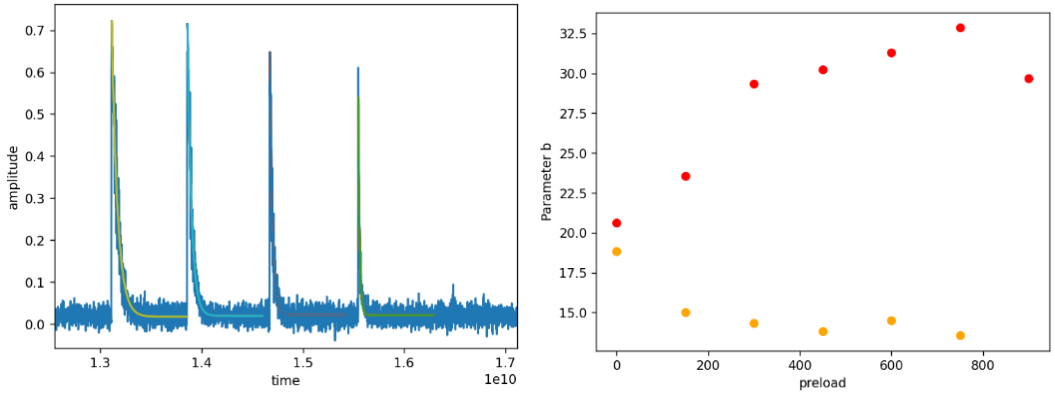

Figure 11: Left - rectified time series of a multiple excitation; Right - decay time evaluation (tensile load red, compressive load orange)

This approach is characterized by poor separability of the load levels, especially in the relevant pressure range, leading to the conclusion that local decay curves have no potential for the main experiments.

4. Ummagentization response (magnetic approx. 50-100 Hz).

When investigating the magnetic response of the bar, an electromagnetic yoke is placed on the side of the bar as shown in Figure 12. This arrangement represents a metrological averaging of the volume of material trapped under the yoke in the magnetic field.

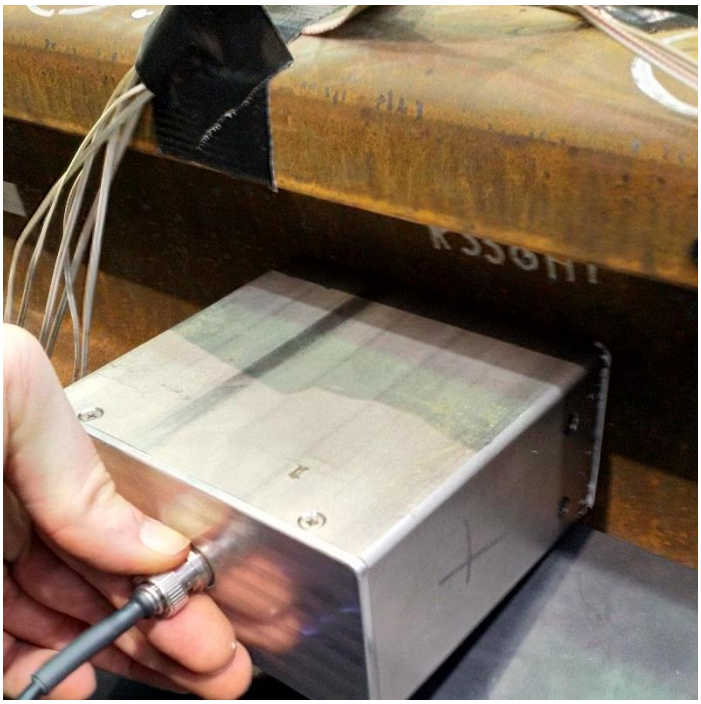

Figure 12: Electromagnetic yoke on the rail web

Based on a voltage impression and current consumption, this test method provides 21 partially physically motivated characteristic values that describe the magnetic hysteresis behavior of the material in detail. However, in order to derive direct correlations to the load, a statistical evaluation is typically performed on the basis of transformation relationships that are aligned with the target variable. In the present case, Figure 13 shows the result for the classification of the compressive load levels applied in the first test.

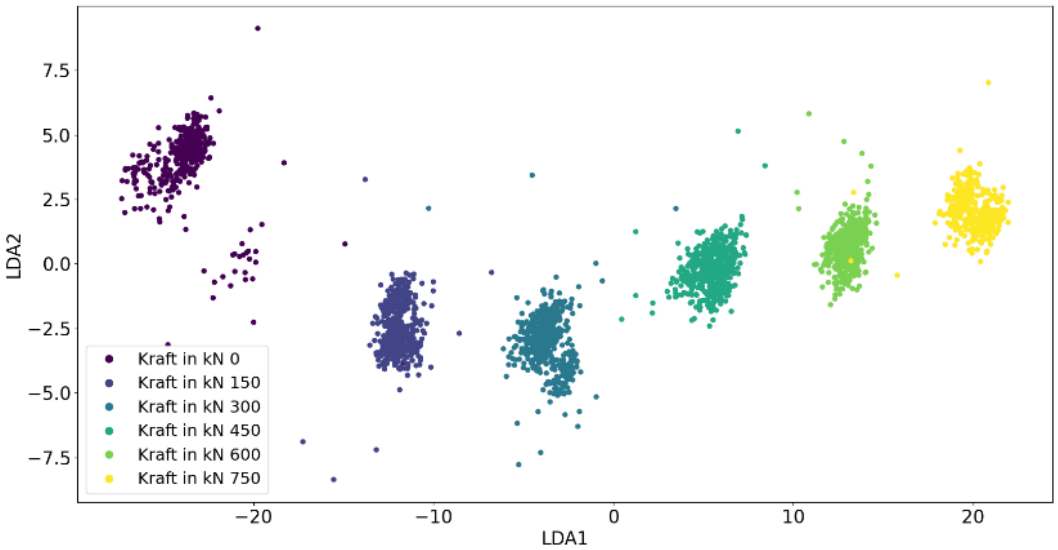

Figure 13: Plot of the transformed results of the remagnetization behavior for different compressive load levels

These results are in line with expectations, but at this stage have not demonstrated their transferability between different samples. For this, the results must be compared on different material and wear conditions in the main tests.

4. Results of the signal analysis and possibilities for interpretation

Compressive and tensile loads between -600 and 600 kN were applied during the main test at the test stand of the Technical University of Munich. In the course of these tests, two main ndt-methods were carried out on two different rail grades, each in a worn and new condition. The change in magnetic parameters was determined analogously to the preliminary test. The ultrasonic measurement was adapted on the basis of the findings from the preliminary test and relocated to the rail head in favor of longer measuring distances for the time-of-flight measurement. Figure *14* shows the new measurement position. In addition, the transmission of long-range structure-borne sound waves was previously evaluated as a possible measurement modality. However, this modality makes demands on the analysis and data processing, the extent of which cannot be estimated at this point in time, especially concerning an adequate way to generate unique signals for precise long-range time-of-flight-analysis.

Figure 14: Ultrasonic test position on the upper side of the rail web

The typical signals, their evaluation and the approach to evaluation are described below.

1. **dependence of characteristic magnetic values on the load in longitudinal direction**

The raw signals of the 21 characteristic quantities are each plotted as a single time series and synchronously related to each other. Figure *15* shows an exemplary plot, which is typically carried out in two or more dimensions. These orders allow later, for example by regression or

KNN algorithms, an assignment of measured values to previously created groups of measured value data sets.

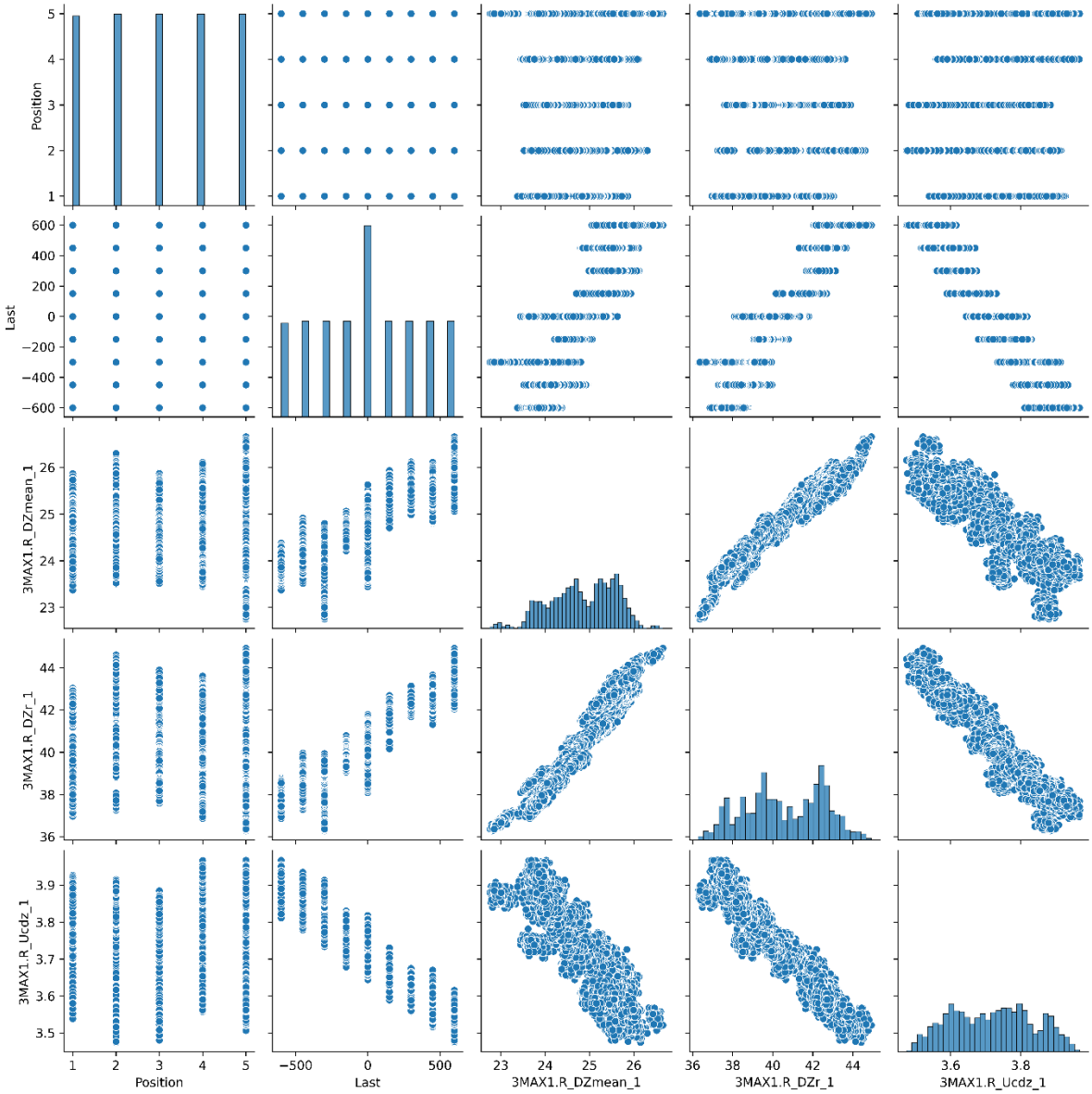

Figure 15: Exemplary pairwise plotting of 3 of 21 parameters of the raw data of rail 4 of the main test

The goal of this approach is to generate a calibration that is as robust as possible with known material and load conditions, allowing larger areas to be covered with a comparative data set. It is expected that the data from the main test will provide a solid basis, but due to the high costs per rail in the preparation and comparison measurement, it is not yet possible to make a comprehensive statement about the required calibration effort in the field. Testing the transferability of the characteristic magnetic changes represents a separate project in the context of later commercial system development.

Result: The multivariate analysis of the results is necessary to achieve a high repeatability of the method at the low absolute stress changes of maximum 200 MPa. For the use of the

method as such, optimized holding devices for the user as well as low test frequencies, can positively influence the reproducibility.

2. **ultrasonic time-of-flight measurement to determine the load stress.**

The determination of the relative change in the propagation speed of the transverse waves is analogous to the approach taken in the web when measuring from the upper side of the rail head. This means that two different wave orientations are generated one after the other with the same electromagnetic transverse wave transducer. The central point of this evaluation is the determination of the time-of-flight of the respective wave, in order to be summarized afterwards to a differential material-stress. This result is significantly influenced by the force in the longitudinal direction due to the lower mechanical inhibition of the rail.

In real measurement, the material, microstructure and reflection conditions pose a great challenge for the mathematical determination of the time-of-flight. Figure 16 shows the measure of similarity between two ultrasonic backwall echoes recorded at an angle of 90 degrees, determined by cross-correlation.

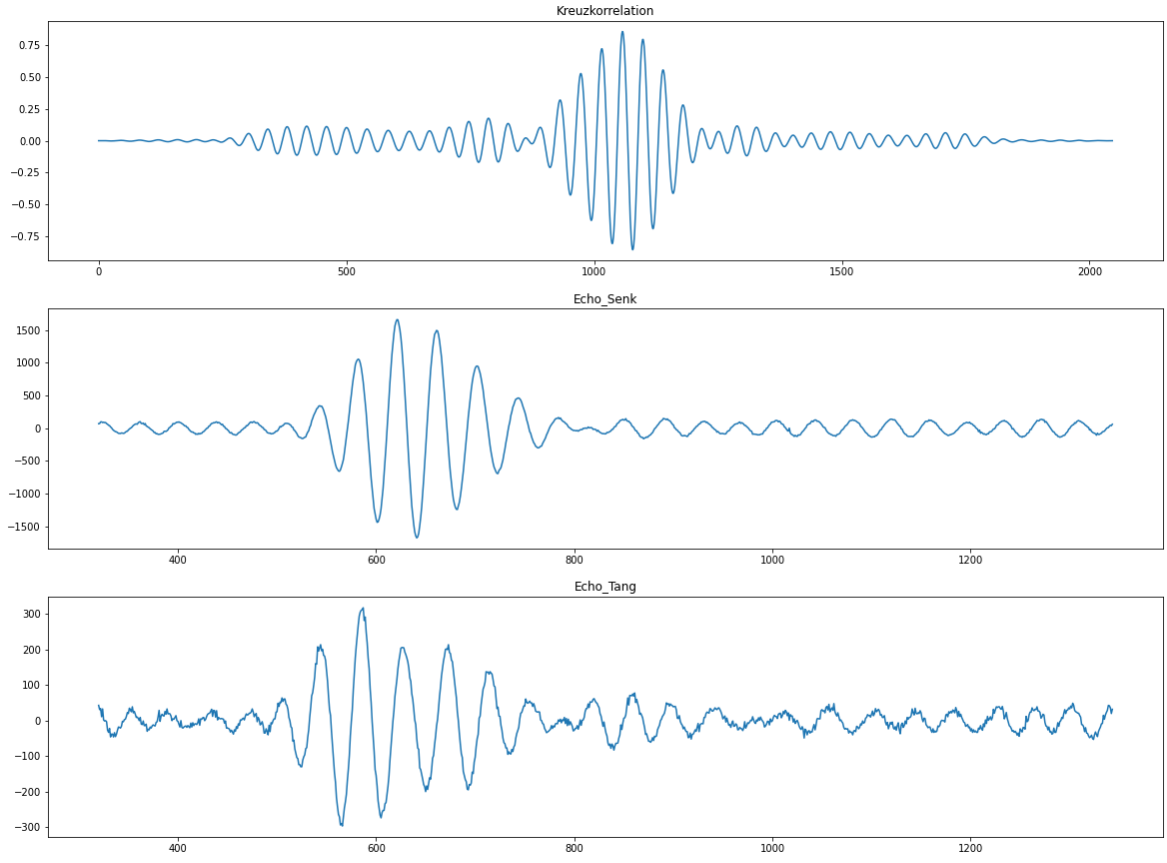

Figure 16: Cross-correlation of two backwall echoes recorded at rail 1 under a load of -300 kN

In the case of the cross-correlated results, a plausibility check is mandatory for the signals, since, assuming sufficiently high signal amplitudes, only a defined time displacement between the two backwall echoes is physically justifiable and mechanically correct. This restriction results from the mechanical as well as acousto-elastic parameters of the material from which the rail is made. With the help of such a test, erroneous measurements can be approximately excluded. Figure *17* and Figure *18* show below how results look with and without plausibility check.

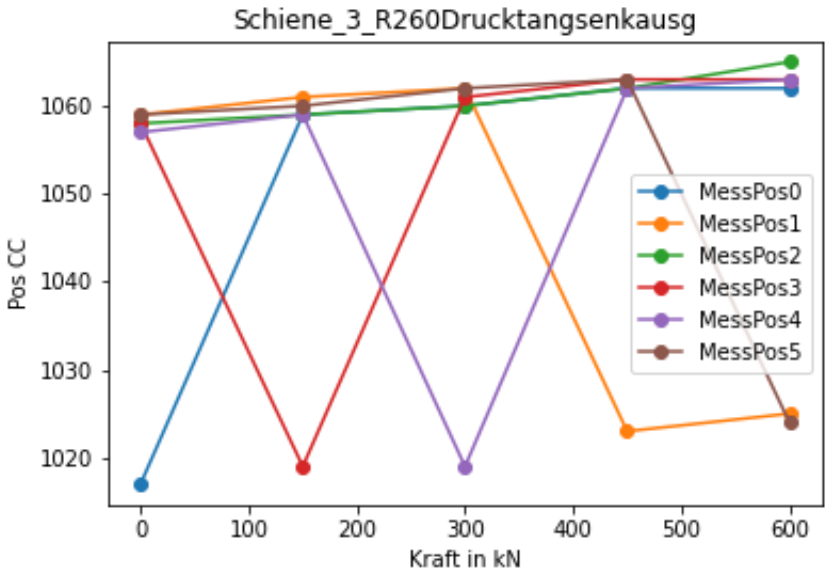

Figure 17: Analysis of the positions of the cross-correlation shift without plausibility check for the test of rail 3

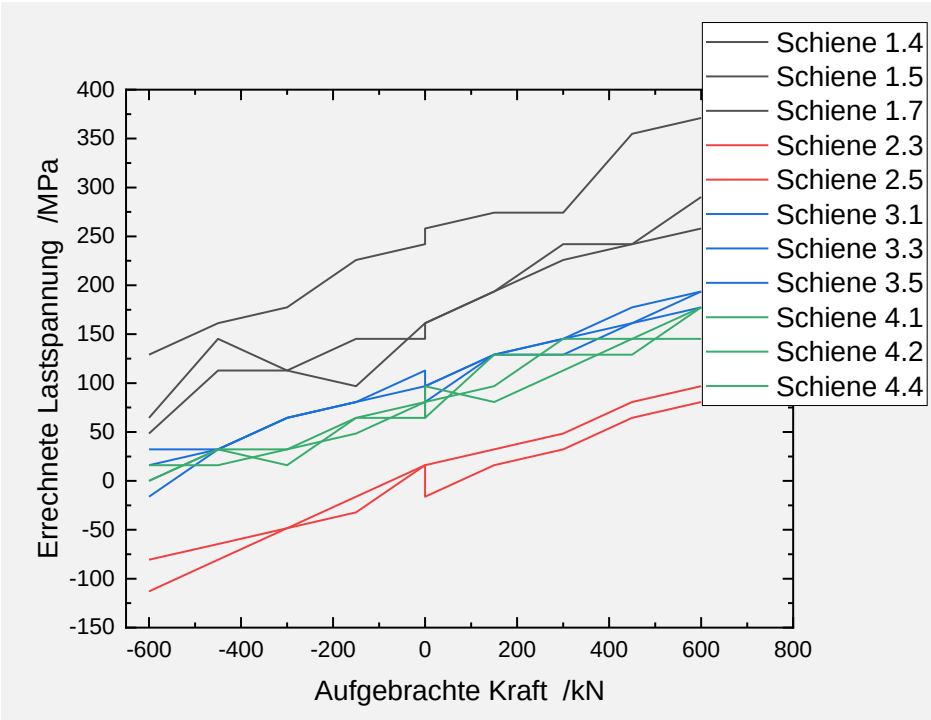

Figure 18: Representation of the applied forces in comparison with the calculated stresses in the cross section of the main test on all 4 rail specimen

Result: Physically implausible signals are detectable within the ultrasonic measurement and can be corrected in parts. However, additional material parameters are required for this. These quantities still have to be determined in general for the different materials within the framework of the economic evaluation. Beyond the actual signal interpretation, the ultrasonic method reveals the requirements with regard to a correction of the prevailing residual stresses along the tested sound path. Different shifts of the calculated results between new and used components of the same type become apparent. This indicates that a consideration of the change in residual

5. Residual Stresses of Selected Rails

For four pre-defined rail specimen of different quality and condition, the residual stress was determined. Therefore, of every rail the cut out of three cross sections was conducted. The designation of these test specimen was as follows:

- Rail 1:R350HT “worn”
- Rail 2:R260 “worn”
- Rail 3:R260 “new”
- Rail 4:R350HT “new”

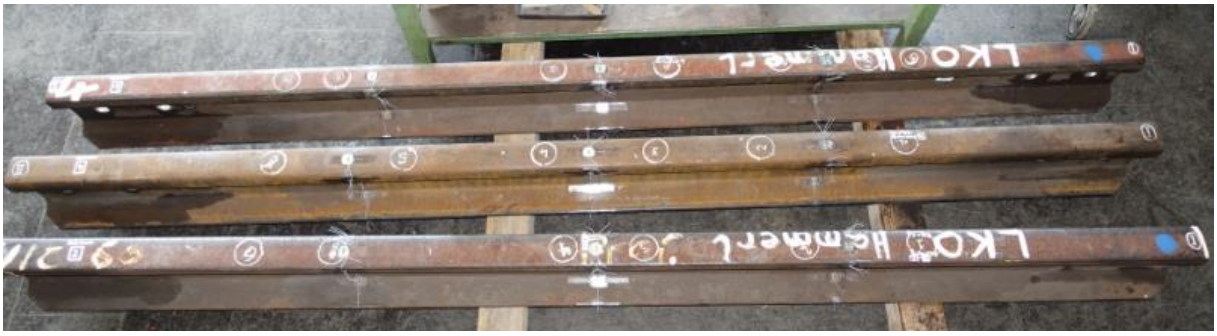

Figure 19: Prepared test specimen for the saw-cutting

With the saw-cutting-method, according to DIN EN 13674-1:2011-04 and DBS 918 254-01 Juli 2017, three cross-sections per rail specimen were cutted out with a band-saw, as can be seen in Figure *24* to Figure *26*. In total, this resulted in 12 cross-sections which have been used for the evaluation of the residual stress.

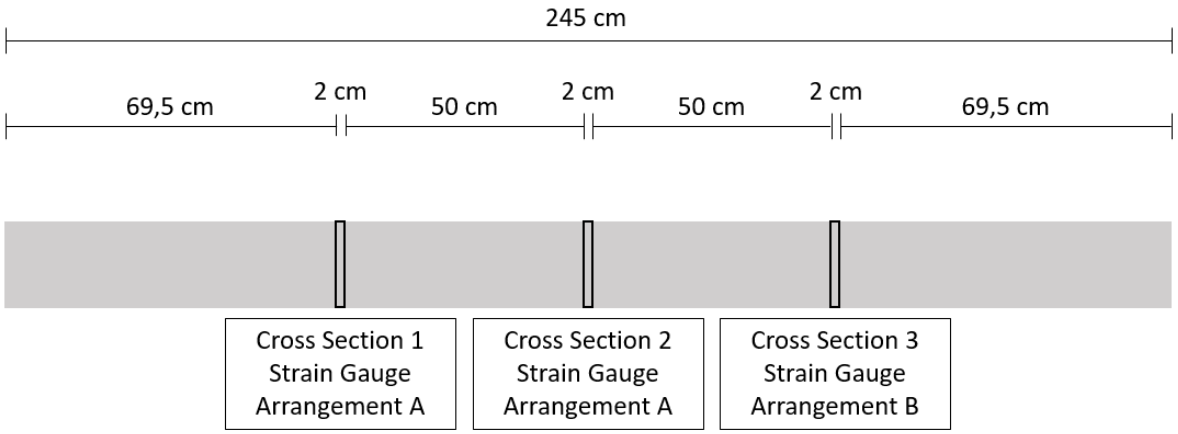

Figure 20: Definition of Cross Sections and Strain Gauge Arrangements

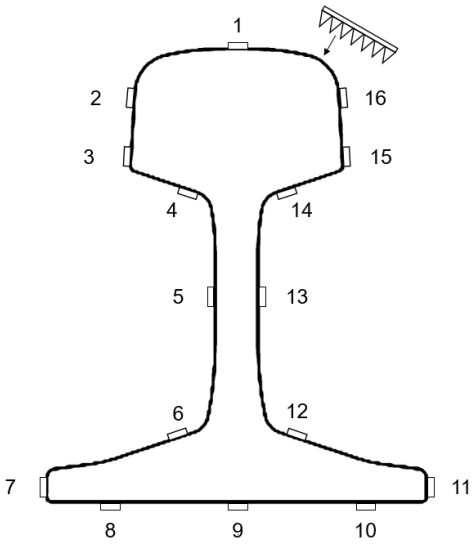

Figure 21: Strain Gauge Arrangement A

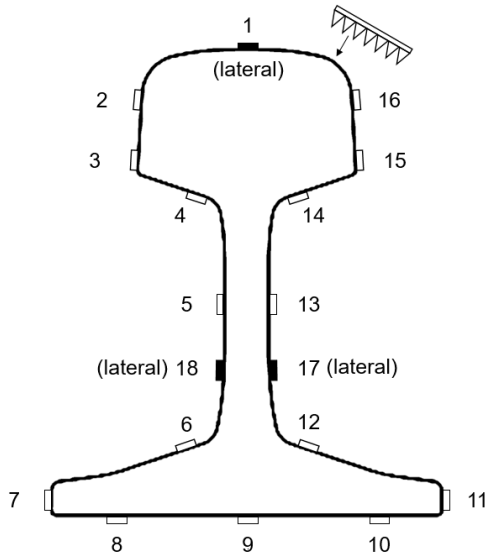

Figure 22: Strain Gauge Arrangement B

Additional to the common arrangement (see Figure *21*) of the strain gauges to investigate the residual stress, every cross-Section 3 of the four rails was modified with strain gauges in order to measure the lateral strain behavior (see Figure *22*). The longitudinal strain gauge 1 was replaced by a lateral strain gauge, two lateral strain gauges 17 and 18 were mounted in addition at the lower part of the rail web between the already existing longitudinal strain gauges 5,6 resp. 12,13.

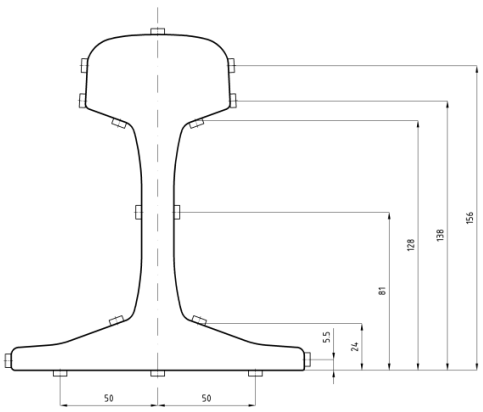

Figure 23: Position of the strain gauges according to DBS 918 254-01

Figure 24: Cutted cross-section with strain gauges still attached

Figure 25: Test specimen and band saw during the cutting

Figure 26: Detailed view of the cutting and strain gauges

5.1. Determination of the longitudinal residual stresses

With the knowledge of the strain development during the cutting of one rail-slice, the residual strain can be calculated according to DIN EN 13674-1 with a young's modulus of 2,07x10^5 MPa and the strain values at the end of the measurement. The strain development was observed several minutes after the last cut, in order to eliminate influences like temperature reduction, which would affect the evaluation.

Diagram *1* shows exemplary the stress development at the 18 strain gauges during the saw cutting of Rail 2 Cross-Section 3. The durations of the two saw-cuts are depicted with two arrows. The time span after the second saw-cut was to ease the temperature back to ambient temperature.

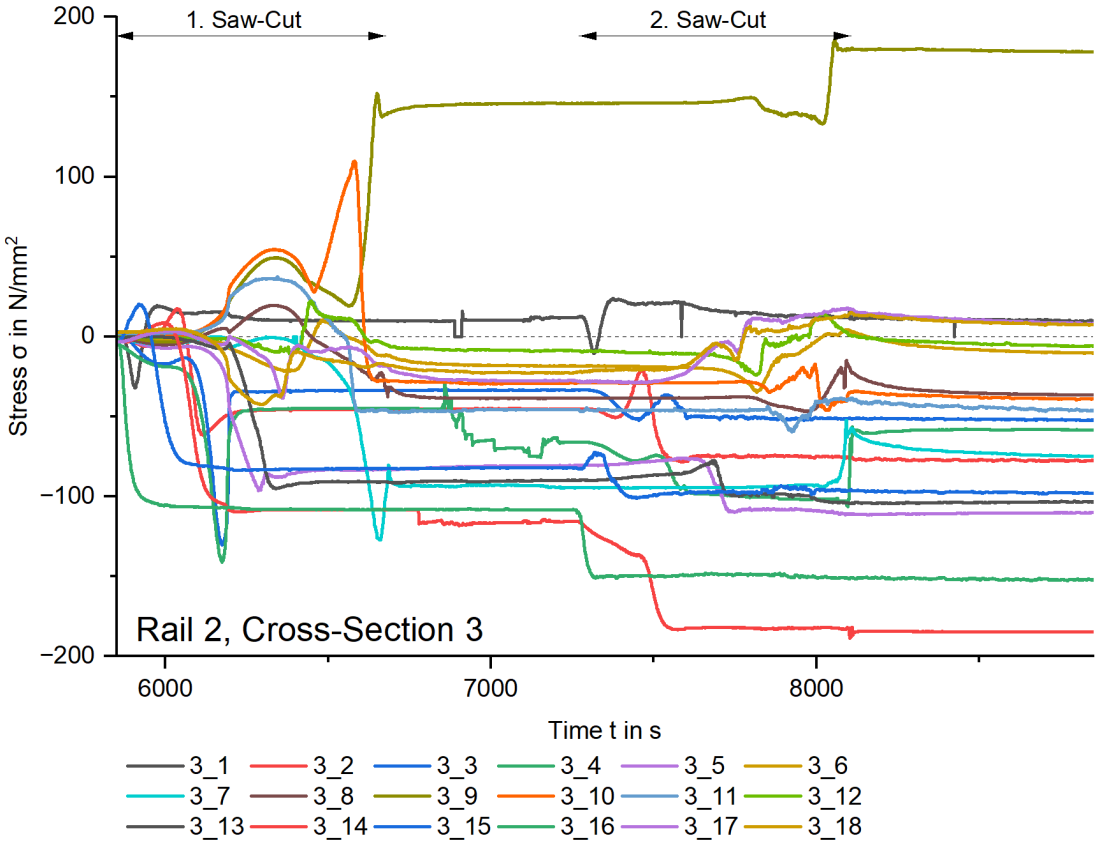

Diagram 1: Stress development of Rail 2 Cross-Section 3

Rail 1 and 2 are worn, the remaining cross-section areas are shown in Figure *27* and Figure *28*. The measurement was conducted with the tool "Calipri C40".

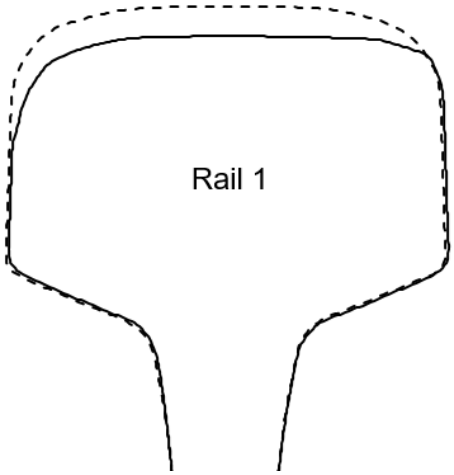

Figure 27: Remaining cross-section of rail 1

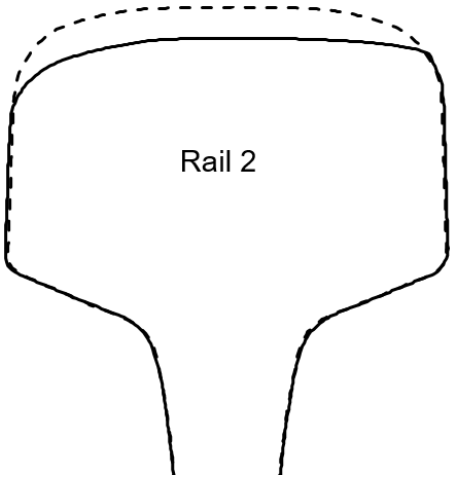

Figure 28: Remaining cross-section of rail 2

5.1.1. Residual strain/stress values in longitudinal direction for Rail 1 R350HT "worn"

Residual strain/stress values in longitudinal direction for Rail 1 R350HT "worn"								
Strain-Gauge #	**Cross-Section 1**		**Cross-Section 2**		**Cross-Section 3**		**Mean value***	
	ε in µm/m	**σ** in MPa	**ε** in µm/m	**σ** in MPa	**ε** in µm/m	**σ** in MPa	**ε** in µm/m	**σ** in MPa
1 (head, upper surface)	827,0	-171,2	722,0	-149,5	n.v.	n.v.	774,5	**-160,3**
2 (head, upper left)	346,0	-71,6	271,3	-56,2	255,6	-52,9	291,0	**-60,2**
3 (head, lower left)	-448,8	92,9	-516,1	106,8	-322,9	66,8	-429,2	**88,9**
4 (transition head/web)	865,2	-179,1	762,7	-157,9	470,5	-97,4	699,5	**-144,8**
5 (web left)	163,6	-33,9	204,9	-42,4	193,0	-39,9	187,2	**-38,7**
6 (trans. web/foot left)	62,6	-13,0	165,6	-34,3	215,6	-44,6	147,9	**-30,6**
7 (foot outer edge left)	231,2	-47,9	322,3	-66,7	203,2	-42,1	252,2	**-52,2**
8 (foot bottom left)	98,9	-20,5	119,1	-24,7	150,2	-31,1	122,8	**-25,4**
9 (foot bottom middle)	-598,7	123,9	-759,3	157,2	-833,7	172,6	-730,6	**151,2**
10 (foot bottom right)	24,0	-5,0	-7,3	1,5	-40,6	8,4	-8,0	**1,7**
11 (foot outer edge right)	143,7	-29,7	216,6	-44,8	290,9	-60,2	217,0	**-44,9**
12 (trans. web/foot right)	33,0	-6,8	106,9	-22,1	145,3	-30,1	95,1	**-19,7**
13 (web right)	193,4	-40,0	239,2	-49,5	271,9	-56,3	234,9	**-48,6**
14 (trans. head/web right)	796,4	-164,9	767,9	-159,0	767,5	-158,9	777,3	**-160,9**
15 (head lower right)	184,0	-38,1	145,8	-30,2	loss	loss	164,9	**-34,1**
16 (head upper right)	546,6	-113,1	559,6	-115,9	553,4	-114,6	553,2	**-114,5**
* positive values = tensile stress negative values = compressive stress								

5.1.2. Residual strain/stress values in longitudinal direction for Rail 2 R260 “worn”

Residual strain/stress values in longitudinal direction for Rail 2 R260 “worn”								
Strain-Gauge #	**Cross-Section 1**		**Cross-Section 2**		**Cross-Section 3**		**Mean value***	
	ε in µm/m	**σ** in MPa	**ε** in µm/m	**σ** in MPa	**ε** in µm/m	**σ** in MPa	**ε** in µm/m	**σ** in MPa
1 (head, upper surface)	917,6	-189,9	1029,5	-213,1	n.v.	n.v.	973,6	**-201,5**
2 (head, upper left)	297,6	-61,6	191,8	-39,7	368,7	-76,3	286,0	**-59,2**
3 (head, lower left)	246,7	-51,1	225,3	-46,6	252,1	-52,2	241,4	**-50,0**
4 (transition head/web)	321,0	-66,5	333,4	-69,0	276,9	-57,3	310,4	**-64,3**
5 (web left)	619,3	-128,2	535,4	-110,8	523,6	-108,4	559,4	**-115,8**
6 (trans. web/foot left)	85,4	-17,7	140,5	-29,1	56,8	-11,8	94,2	**-19,5**
7 (foot outer edge left)	591,5	-122,4	636,6	-131,8	366,7	-75,9	531,6	**-110,0**
8 (foot bottom left)	53,5	-11,1	144,9	-30,0	176,3	-36,5	124,9	**-25,9**
9 (foot bottom middle)	-977,3	202,3	-1008,3	208,7	-845,6	175,0	-943,7	**195,4**
10 (foot bottom right)	117,8	-24,4	186,4	-38,6	190,6	-39,4	164,9	**-34,1**
11 (foot outer edge right)	368,0	-76,2	223,8	-46,3	228,7	-47,3	273,5	**-56,6**
12 (trans. web/foot right)	loss	loss	85,1	-17,6	35,9	-7,4	60,5	**-12,5**
13 (web right)	508,1	-105,2	458,9	-95,0	490,3	-101,5	485,8	**-100,6**
14 (trans. head/web right)	685,7	-141,9	764,5	-158,3	880,3	-182,2	776,8	**-160,8**
15 (head lower right)	370,3	-76,6	284,5	-58,9	469,2	-97,1	374,7	**-77,6**
16 (head upper right)	715,7	-148,1	loss	loss	727,0	-150,5	721,4	**-149,3**
* positive values = tensile stress negative values = compressive stress								

5.1.3. Residual strain/stress values in longitudinal direction for Rail 3 R260 "new"

Residual strain/stress values in longitudinal direction for Rail 3 R260 "new"								
Strain-Gauge #	**Cross-Section 1**		**Cross-Section 2**		**Cross-Section 3**		**Mean value***	
	ε in µm/m	**σ** in MPa	**ε** in µm/m	**σ** in MPa	**ε** in µm/m	**σ** in MPa	**ε** in µm/m	**σ** in MPa
1 (head, upper surface)	loss	loss	-520,0	107,6	n.v.	n.v.	-520,0	**107,6**
2 (head, upper left)	loss	loss	56,4	-11,7	48,1	-10,0	52,3	**-10,8**
3 (head, lower left)	loss	loss	-21,9	4,5	-14,4	3,0	-18,2	**3,8**
4 (transition head/web)	loss	loss	314,9	-65,2	338,2	-70,0	326,6	**-67,6**
5 (web left)	loss	loss	566,0	-117,2	574,6	-119,0	570,3	**-118,1**
6 (trans. web/foot left)	loss	loss	-52,6	10,9	-55,4	11,5	-54,0	**11,2**
7 (foot outer edge left)	loss	loss	402,3	-83,3	loss	loss	402,3	**-83,3**
8 (foot bottom left)	loss	loss	-78,0	16,1	-74,9	15,5	-76,4	**15,8**
9 (foot bottom middle)	loss	loss	-365,0	75,6	-366,5	75,9	-365,8	**75,7**
10 (foot bottom right)	loss	loss	loss	loss	-43,4	9,0	-43,4	**9,0**
11 (foot outer edge right)	loss	loss	515,0	-106,6	522,9	-108,2	518,9	**-107,4**
12 (trans. web/foot right)	loss	loss	-33,8	7,0	-35,2	7,3	-34,5	**7,1**
13 (web right)	loss	loss	533,8	-110,5	520,3	-107,7	527,0	**-109,1**
14 (trans. head/web right)	loss	loss	393,8	-81,5	435,4	-90,1	414,6	**-85,8**
15 (head lower right)	loss	loss	-395,5	81,9	-413,2	85,5	-404,4	**83,7**
16 (head upper right)	loss	loss	-633,6	131,2	-680,7	140,9	-657,2	**136,0**
* positive values = tensile stress negative values = compressive stress								

5.1.4. Residual strain/stress values in longitudinal direction for Rail 4 R350HT "new"

Residual strain/stress values in longitudinal direction for Rail 4 R350HT "new"								
Strain-Gauge #	**Cross-Section 1**		**Cross-Section 2**		**Cross-Section 3**		**Mean value***	
	ε in µm/m	**σ** in MPa	**ε** in µm/m	**σ** in MPa	**ε** in µm/m	**σ** in MPa	**ε** in µm/m	**σ** in MPa
1 (head, upper surface)	-1207,7	250,0	-1141,4	236,3	n.v.	n.v.	-1174,6	**243,1**
2 (head, upper left)	213,9	-44,3	194,5	-40,3	212,5	-44,0	207,0	**-42,8**
3 (head, lower left)	-486,4	100,7	-506,9	104,9	-464,1	96,1	-485,8	**100,6**
4 (transition head/web)	646,0	-133,7	639,2	-132,3	633,0	-131,0	639,4	**-132,4**
5 (web left)	98,3	-20,3	88,3	-18,3	92,9	-19,2	93,2	**-19,3**
6 (trans. web/foot left)	-31,9	6,6	-54,9	11,4	-73,6	15,2	-53,5	**11,1**
7 (foot outer edge left)	219,6	-45,5	256,5	-53,1	214,8	-44,5	230,3	**-47,7**
8 (foot bottom left)	-94,7	19,6	-81,7	16,9	-97,8	20,3	-91,4	**18,9**
9 (foot bottom middle)	-701,9	145,3	-721,6	149,4	-719,2	148,9	-714,2	**147,9**
10 (foot bottom right)	-114,1	23,6	-87,1	18,0	-97,5	20,2	-99,6	**20,6**
11 (foot outer edge right)	181,0	-37,5	217,8	-45,1	176,6	-36,6	191,8	**-39,7**
12 (trans. web/foot right)	-34,9	7,2	-56,3	11,7	-44,5	9,2	-45,3	**9,4**
13 (web right)	86,5	-17,9	77,0	-15,9	105,2	-21,8	89,6	**-18,5**
14 (trans. head/web right)	646,6	-133,8	633,9	-131,2	746,6	-154,5	675,7	**-139,9**
15 (head lower right)	-442,7	91,7	-455,2	94,2	-432,2	89,5	-443,4	**91,8**
16 (head upper right)	-2,3	0,5	-9,0	1,9	-26,1	5,4	-12,5	**2,6**
* positive values = tensile stress negative values = compressive stress								

5.2. Determination of the lateral strain/stress for selected locations

In addition to the determination of the longitudinal residual strain/stress, also the lateral strain/stress was investigated for a selected location of every cross-section 3. The procedure is the same as with the lateral strain gauges. It is calculated with a young's modulus of $2{,}07 \times 10^5$ MPa according to DIN EN 13674-1. The strain development was observed several minutes after the last cut, in order to eliminate influences like temperature reduction, which would affect the evaluation.

Residual strain/stress values in lateral direction								
Strain-Gauge #	**Rail 1 R350HT "worn" Cross-Section 3**		**Rail 2 R260 "worn" Cross-Section 3**		**Rail 3 R260 "new" Cross-Section 3**		**Rail 4 R350HT "new" Cross-Section 3**	
	ε in µm/m	**σ** in MPa	**ε** in µm/m	**σ** in MPa	**ε** in µm/m	**σ** in MPa	**ε** in µm/m	**σ** in MPa
1 (head, upper surface)	206,0	-42,6	-38,7	8,0	302	-62,5	589,8	-122
17 (web lower left)	Drift	Drift	-29,5	6,1	-3,0	0,6	Drift	Drift
18 (web, lower right)	Drift	Drift	-31,6	6,5	-8,6	1,8	Loss	Loss
* positive values = tensile stress negative values = compressive stress								

5.3. Additional Information: Temperature development while cutting

As additional information, the temperature of the rail was observed with a thermal imaging camera (Fluke TiS 55) during the saw cutting and immediately after the cut, so that the maximum temperature rise was figured out.

Figure *29* to Figure *31* show exemplary for every single saw-cut the temperature distribution in the rail profile. After the first cut, a maximum temperature of about 49.6°C can be observed. With the second saw cut, the temperature increases up to 64.7°C at the rail foot. The residual stress evaluation is unimpaired of the temperature developed during the saw-cuts, since the measurement maintained long enough after the last cut.

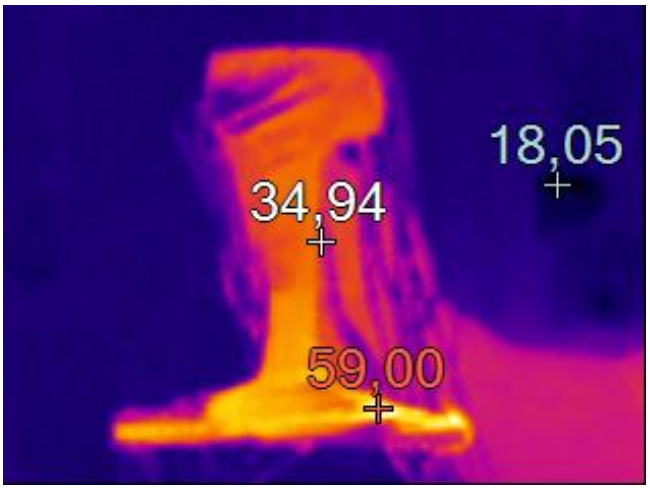

Rail 1 Cross-Section 1 after 2nd saw-cut

T_{min} = 34,94 °C

T_{max} = 59,00 °C

Assumed emissivity = 0,70

Figure 29: Rail 1 Cross-Section 1 after 2nd Saw-Cut

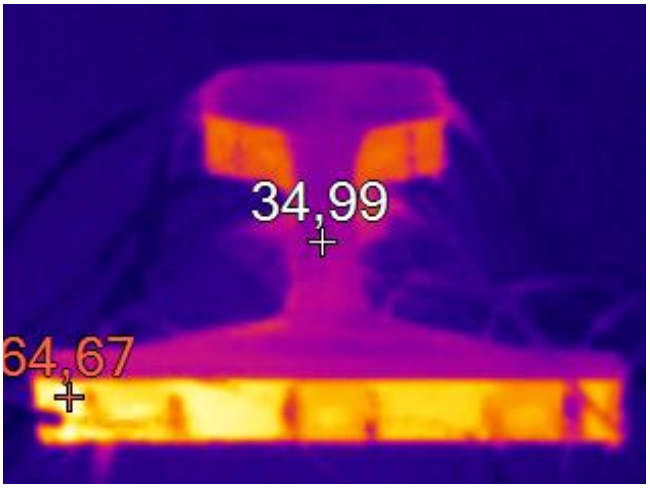

Rail 1 Cross-Section 2 after 2nd saw-cut

T_{min} = 34,99 °C

T_{max} = 64,67 °C

Assumed emissivity = 0,70

Figure 30:Rail 1 Cross-Section 2 after 2nd saw-cut

Rail 4 Cross-Section 3 after 1st saw-cut

T_{min} = 24,13 °C

T_{max} = 49,60 °C

Assumed emissivity = 0,70

Figure 31: Rail 4 Cross-Section 3 after 1st Saw-Cut

END OF REPORT D2.3.2